Synthesis of Single-Crystalline Gold Nanoplates in Aqueous Solutions through Biomineralization by Serum Albumin Protein

Jianping Xie,[†] Jim Yang Lee,*[,†,‡] and Daniel I.C. Wang[†,§]

Singapore−MIT Alliance, 4 Engineering Drive 3, National University of Singapore, Singapore 117576, Department of Chemical Engineering, Massachusetts Institute of Technology, 77 Massachusetts Avenue, Cambridge, Massachusetts 02139, and Department of Chemical and Biomolecular Engineering, National University of Singapore, 10 Kent Ridge Crescent, Singapore 119260

Received: March 11, 2007; In Final Form: May 14, 2007

In this work, single-crystalline gold nanoplates were produced by reacting an aqueous solution of chloroauric acid with one serum albumin protein (BSA) at the physiological temperature, where BSA provided the dual function of Au(III) reduction and directing the anisotropic growth of Au(0) into plate-like structures. Structural characterizations by FESEM, TEM, HRTEM, and SAED showed that the nanoplates were oriented with {111} planes as their basal planes. The effects of environmental factors such as temperature and pH were investigated, which showed low temperature and acidic pH favoring the anisotropic growth of gold nanoparticles. More interestingly, the kinetics of chloroauric acid reduction in BSA solutions could be manipulated through the addition of a trace amount of Ag^+ ions, and plates with lateral size ranging from a few micrometers to tens of nanometers could be produced. The growth of gold nanoplates in BSA solution with time was monitored by electron microscopy, allowing the detection of several key intermediate structures in the growth process.

Introduction

There has been increased emphasis on the development of clean synthetic procedures ("green chemistry")[1] in the pursuit of nanotechnology, especially for nanoproducts targeted at bioapplications. The selection of an environmentally acceptable solvent system, an eco-friendly reducing agent and a nonhazardous capping agent for the stabilization of the nanoparticles are three criteria for a totally "green" nanoparticle synthesis. The synthesis of nanoparticles by microorganisms[2] or biomolecules[3] is ideal according to these criteria.

Recent interest in nanomaterials is founded on size and shape tunable properties which allow very diverse applications to be designed based on the same material.[4] This has led to the empirical discovery of various methods for the control of nanoparticle morphology. Insofar as gold is concerned, although there has been a large volume of work on the synthesis of zero dimension (0D) nanospheres[4c] and 1D nanorods[5] by chemical methods, there have been relatively few attempts to produce plate-like 2D gold nanostructures. According to published literature, gold nanoplates can be synthesized by photochemical,[6] solution chemistry,[7] and biochemical methods.[2,8] When compared with the synthesis of silver nanoplates where edge length[9] and thickness[10] are controllable to some extent, the high yield synthesis of gold nanoplates with control of the edge length and thickness is still a challenge. In our recent work on the high-yield synthesis of single-crystalline gold nanoplates using a multicellular brown seaweed,[2] proteins were implicated as the primary active biomolecules involved in the reduction of chloroaurate ions and the growth of Au nuclei into gold nanoplates. Functional groups such as carboxyl, hydroxyl, amine, and thiol which are abundant in proteins could be the possible sites of action. The activity of proteins and the contributions from these functional groups may be demonstrated more aptly with the use of a well-studied protein.

Herein we report the use of a globular protein, bovine serum albumin (BSA), for the synthesis of planar gold nanostructures through simple changes of the experimental conditions. BSA is the most abundant plasma protein and a model globular protein that is widely used in bionanotechnology applications such as sensing, self-assembly and imaging.[11] Previous studies on protein−Au ion interactions have focused on elucidating the damage inflicted by anticancer Au(III) complexes on proteins.[12] Marcon et al.[12] investigated the reactions of six such Au(III) complexes with BSA, and found two of them to undergo progressive reduction in the presence of BSA. In this study, a common Au(III) complex, $HAuCl_4$, was used instead to evaluate the biomineralization ability of BSA. The experimental results revealed that the serum albumin is a multifunctional biomacromolecule; i.e., it not only reduced the chloroaurate ions but also directed the oriented growth of gold nanocrystals. Triangular and hexagonal gold nanoplates were obtained by the BSA reduction of chloroaurate ions under mild conditions. This is perhaps the first work on the synthesis of gold nanoplates with good yield using a single commercially available protein as reducing *cum* shape-directing agent. The effects of environmental factors such as temperature and pH of the reaction medium on particle shape and size were systematically studied. A new size-controlled process was developed by introducing a trace amount of silver ions to modulate the kinetics of chloroaurate ion reduction to form regular triangular and hexagonal nanoplates with widths from a few micrometers to tens of nanometers. The growth of gold nanoplates was

* Corresponding author. Fax: +65 6779 1936. Tel: +65 6874 2899. E-mail: cheleejy@nus.edu.sg.
[†] Singapore−MIT Alliance, National University of Singapore.
[‡] Department of Chemical and Biomolecular Engineering, National University of Singapore.
[§] M.I.T.

10.1021/jp0719715 CCC: $37.00
Published on Web 06/22/2007

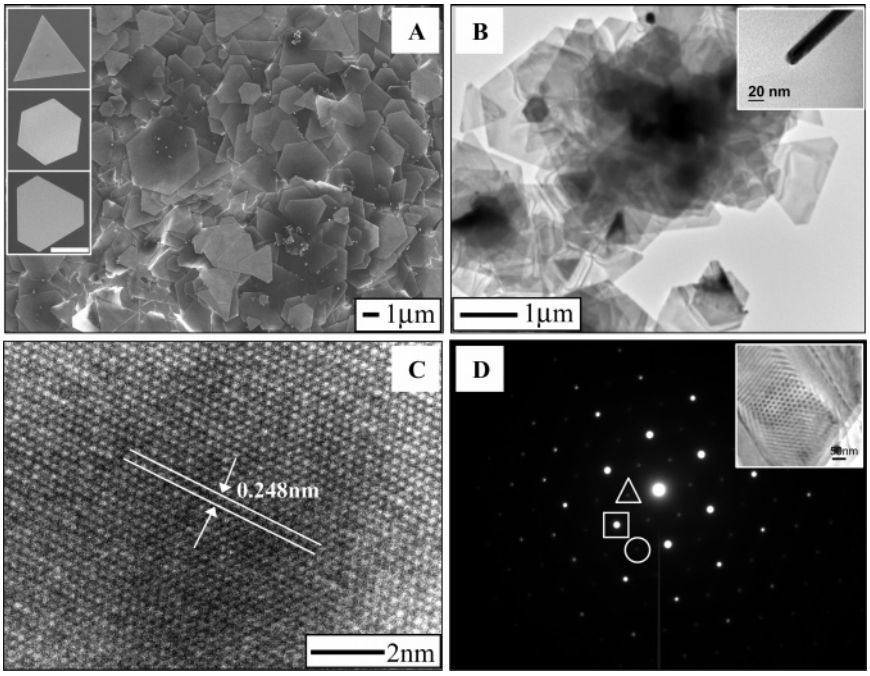

Figure 1. (A, B) Representative FESEM and TEM images of gold nanoplates synthesized by the reduction of $AuCl_4^-$ in BSA solution. The inset in panel A shows three types of gold nanoplates: triangular, hexagonal, and truncated triangular. The inset in panel B shows a gold nanoplate standing perpendicularly to the TEM grid, which allowed the precise measurement of its thickness. (C) HRTEM image from the vertex of a gold nanoplate. (D) SAED pattern from a gold nanoplate. The boxed spots, circled spots, and spots circumscribed by triangles correspond to {220}, {422}, and 1/3{422} diffractions, respectively. The inset shows two typical Moire patterns formed by stacking two or more nanoplates against their triangular faces. Synthesis conditions: BSA (1 mL, 10 mg/mL) + deionized water (8 mL) + $HAuCl_4$ (1 mL, 10 mM); initial pH 3.2, 37 °C for 48 h.

reconstructed by following the shape and size evolution of the product particles. Presented below are the details of this investigation.

Experimental Section

All chemicals were purchased from Sigma Aldrich and used as received. Ultrapure Millipore water (18.2MΩ) was used as the solvent. All glassware was washed with aqua regia (HCl: HNO_3 in 3:1 ratio by volume), and rinsed with ethanol and ultrapure deionized water. In a typical experiment, 1 mL 10 mM BSA was mixed with 8 mL deionized water, followed by the addition of 1 mL 10 mM $HAuCl_4$ solution, which resulted in an initial pH of 3.2. The pH of the reaction mixture was adjusted to the desired values by adding 1M NaOH solution or 1M HNO_3 solution. The reaction was carried out under vigorous stirring in a water bath at the physiological temperature (37 °C) for 0−48 h. Examinations of nanoparticle morphology and size by field emission scanning electron microscopy (FESEM) and by transmission electron microscopy (TEM) made use of a JEOL JSM-6700F microscope at 25 kV, and a JEOL JEM-2010 microscope at 200kV (or a JEOL JEM 2010FE at 200kV for high-resolution images), respectively. UV−vis spectroscopy and X-ray photoelectron spectroscopy (XPS) were carried out on a Shimadzu UV-2450 spectrometer operating at 1 nm resolution, and on a VG ESCALAB MKII spectrophotometer. Narrow-scan XPS spectra of Au 4f and Ag 3d core levels were deconvoluted by the XPSPEAK (version 4.1) software, using adventitious carbon to correct the binding energy (BE) of C1s to 284.5 eV.

Results and Discussion

Serum albumin is one of the most extensively studied proteins. It is also the most abundant protein in plasma present at a typical concentration of 5 g/100 mL.[13] Bovine serum albumin, with molecular weight of 66 430 Da, is a single polypeptide chain with 583 amino acid residues and no carbohydrates (see Table S1 for the amino acid makeup of BSA[14]). Its secondary structure is highly α-helical.[13] The tertiary structure of BSA consists of three homologous domains (domains I−III), with cysteine residues forming disulfide bonds to produce a double-loop bridging pattern.[15] Several amino acid residues of BSA have sulfur-, oxygen-, and nitrogen-bearing groups which can potentially reduce chloroaurate ions and adsorb on the nanoparticle surface. Recent reports[16] have shown that single amino acids such as l-tryptophan, l-tyrosine, l-arginine, l-lysine, and l-aspartic acid could substitute for citric acid in the citric synthesis of gold nanoparticles. Hence, the reducing ability of BSA is not at all unexpected since it contains more than 100 residues of the abovementioned amino acids, which may provide the electrons required for chloroaurate ion reduction.

1. Gold Nanoplates Synthesized in BSA Solution. The mixture of BSA and aqueous $HAuCl_4$ solution changed color from yellow to reddish brown after 48h. Such color transition is usually indicative of changes in the metal oxidation state. In this case, Au(III) was reduced to Au(0) by BSA in the solution (see Figure S1A for the XPS analysis of the sample, which clearly indicated the formation of zerovalent gold).

Typical FESEM and TEM images showing the size and morphology of gold nanoplates are given in Figure 1A,B. The nanoplates, which were 0.6−3 μm in size along their longest edge and ∼19 nm in thickness (measured from the inset in Figure 1B and confirmed by AFM measurements (data not shown)) were either triangular, truncated triangular or hexagonal in geometry with very smooth edges. As shown in Figure 1A,B, the main products were planar nanoparticles, which accounted for 80% (from counting 100 nanoparticles) of the total nanoparticles synthesized, with the remaining 20% being spherical

TABLE 1: Summary of Experimental Factors and Product Morphologies

environmental factors		time for complete reaction	product morphology
reaction temperature	37 °C	48 h	plates (∼80%) and particles
	70 °C[a]	2 h	plates (∼5%) and particles
	100 °C[b]	0.5 h	aggregated particles
pH[c]	3.2	48 h	plates (∼80%) and particles
	7.3	10 h	particles
	10.9	10 h	particles
$AgNO_3$ concentration[d]	0	48 h	plates (∼80%, 2.1 ± 0.6 μm)
	1 μM	24 h	plates (∼70%, 590 ± 110 nm)
	5 μM	10 h	plates (∼60%, 205 ± 55 nm)
	10 μM	6 h	plates (∼50%, 91 ± 22 nm)
	50 μM	3 h	plates (∼15%, 41 ± 10 nm)

[a] Deionized water (8 mL) + $HAuCl_4$ (1 mL, 10 mM), 70 °C for 10 min, and then 1 mL 10 mg/mL BSA was added, pH 3.2. [b] Deionized water (8 mL) + $HAuCl_4$ (1 mL, 10 mM), boiled for 10 min, and then 1 mL 10 mg/mL BSA was added, pH 3.2. [c] BSA (1 mL, 10 mg/mL) + deionized water (8 mL) + $HAuCl_4$ (1 mL, 10 mM), 37 °C under different initial pH. [d] BSA (1 mL, 10 mg/mL) + deionized water (8 mL) + $HAuCl_4$ (1 mL, 10 mM) + $AgNO_3$ (0, 1 μL, 5 μL, 10 μL, 50 μL; 10 mM), pH 3.2, 37 °C.

gold nanoparticles. Figure 1C shows a typical high-resolution TEM (HRTEM) image of the vertex of an isolated triangular gold nanoplate. The well-resolved interference fringe patterns attest to the single crystallinity of this gold nanoplate. The fringes with a spacing of 0.248 nm could be assigned to 3 × {422} lattice spacing of the face-centered cubic (fcc) gold crystal.[17] The single-crystalline nature of the nanoplates was further confirmed by their electron diffraction patterns (Figure 1D). The SAED pattern, which was obtained by aligning the electron beam perpendicular to the triangular face of a selected nanoplate, shows hexagonally arranged diffraction spots with 6-fold symmetry characteristic of (111)-oriented single-crystal gold nanoplates.[2,7,8] Previous studies of planar structures (such as thin films grown on various substrates) often showed Moire patterns in the TEM images.[18] In our case, the Moire patterns were produced when two or more nanoplates were stacked against each other with good contact of their triangular faces. The inset in Figure 1D shows two typical examples of the Moire patterns: one was an array of parallel lines, and the other was a periodic array of dots. The formation of these patterns can be attributed to the difference in orientation between the two stacked gold nanoplates.

2. Environmental Factors in Synthesis. The formation of gold nanoplates can be attributed to the mild reducing power of BSA, which gave rise to slow reduction kinetics. The environmental factors in the synthesis such as reaction temperature and pH, could significantly affect the reduction and capping capability of BSA and hence the reduction kinetics, the nucleation and the crystal growth of gold nanoparticles. A series of experiments was therefore carried out to determine the effects of these experimental variables on the shapes of the as-synthesized nanomaterials. The results are summarized in Table 1.

Effect of Reaction Temperature. Temperature is expected to influence strongly the conformation of the BSA molecules (and hence the capping capability of BSA), the kinetics of gold ion reduction, and the crystal growth of gold nanoparticles. We carried out the reaction at different temperatures and found that BSA at room-temperature had no apparent reduction capability (no particles were formed even after 2days). The temperature was therefore set at the physiological temperature (37 °C) to provide reasonable reduction kinetics (reaction completion within 2 days). For reactions above 37 °C, the reaction rate increased sharply with temperature, as indicated by the rapidity in the change of the solution color from yellow to purple.

Figure 2A,B are TEM images of gold nanoparticles obtained at 70 and 100 °C, which show that a mild temperature (37 °C) was preferable for the formation of plate-like structures. The yield of nanoplates decreased noticeably with temperature, from 80% at 37 °C to 5% at 70 °C and 0% at 100 °C. The products at 100 °C were predominantly a mixture of aggregated structures with a few spherical and irregular nanoparticles.

The different morphologies from syntheses at different temperatures could also be witnessed by the changes in the UV−vis spectra of the nanoparticles (Figure 2E). It is well-known that the optical properties of metal nanoparticles are strongly size and shape dependent. According to the Mie theory,[19] small spherical nanocrystals (e.g., Ag or Au) should exhibit only a single surface plasmon resonance (SPR), whereas anisotropic particles would have two to three SPR, depending on their shape. The absorption spectrum of gold nanoplates synthesized at 37 °C (spectrum 1) shows one SPR band centering at 530 nm and very broad absorption in the near-IR region typical of the out-of-plane quadrupole resonance and the in-plane dipole resonances respectively.[9] As there existed three types of nanoplates over a range of sizes, the in-plane dipole plasmon absorption band of the sample was naturally broadened. The absorption spectra of gold nanoparticles synthesized at 70 °C (spectrum 2) and 100 °C (spectrum 3) show only a lone absorption peak characteristic of spherical gold nanoparticles at ∼550 nm and ∼540 nm respectively.

Effect of pH. The gold nanoparticles obtained with BSA at different pH were analyzed by TEM. As shown in Figure 1A&B, the primary products formed under acidic conditions were planar nanoparticles (∼80%). At neutral and alkaline pH, spherical gold nanoparticles were formed exclusively, as shown in Figure 2C,D, which was also evident in the UV−vis analysis of the as-synthesized gold nanoparticles (only one absorption peak centering at ∼520 nm was found in spectra 4 and 5 of Figure 2E). Since chloroauric acid is hydrolyzable to hydrated gold oxides in alkaline solution,[20] the oxidation state of the gold nanoparticles formed at pH 10.9 was determined. Clear evidence for the presence of atomic gold was provided by SAED and XPS analyses. The SAED pattern (inset in Figure 2C) in this case shows that the gold nanoparticles were crystalline and randomly oriented. The electron diffraction pattern could be indexed to the fcc structure of gold. The $Au4f_{7/2}$ core level signal in the XPS spectra (see Figure S1B) could be deconvoluted into two chemically distinct components with binding energies of 83.8 and 84.6 eV corresponding to Au(0) and Au(I), respectively.[21] The presence of a small amount of Au(I) (∼7%) on the gold surface was therefore confirmed. It is believed that Au(I) could stabilize the particles electrostatically against aggregation in solution.[22]

The gold nanoparticles synthesized at alkaline pH were mostly spherical, with smaller particle size and narrower size distribution (14.2 ± 1.1 nm) than those of the gold nanoparticles synthesized at neutral pH (15.3 ± 3.6 nm). These trends can be related to the changes in the conformation of the BSA structure with changing pH. BSA undergoes five isomeric conformations with changes in pH.[13] It is present in the normal form at neutral pH, and changes its conformation to the basic form at alkaline pH, which involves the unfolding of domain I and domain III.[13] The unfolding is expected to facilitate the

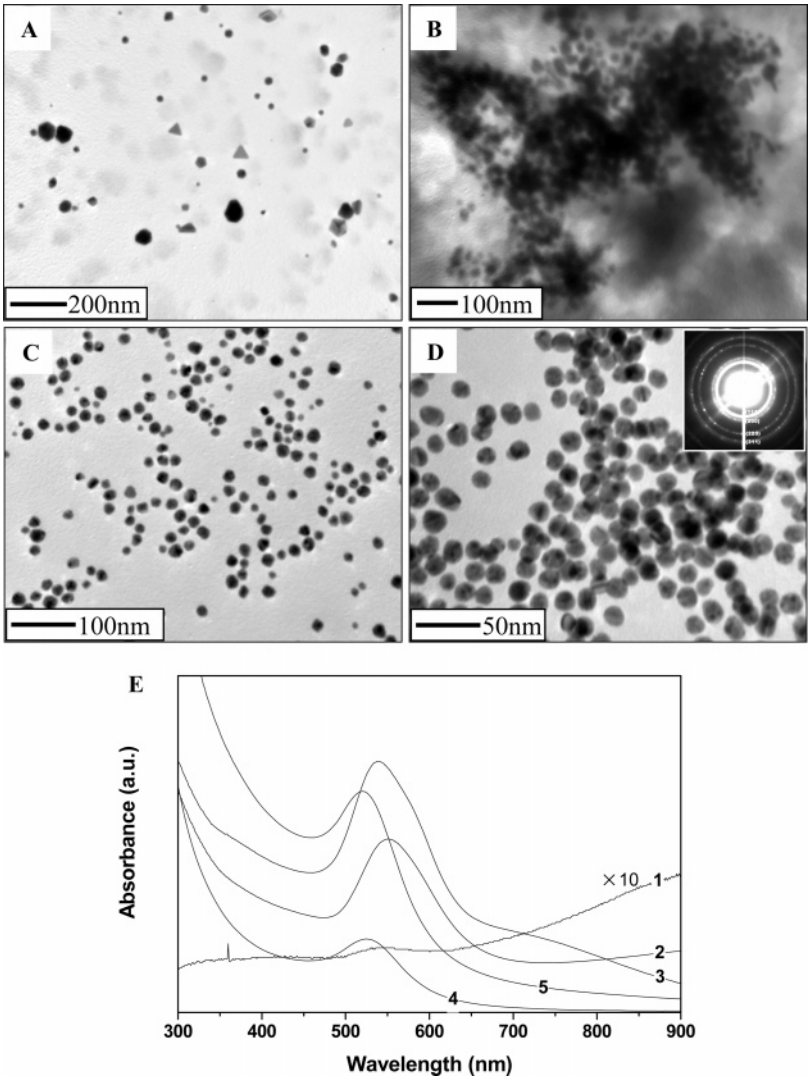

Figure 2. Representative TEM images showing the effects of temperature and pH on product morphology: (A) pH 3.2, 70 °C; (B) pH 3.2, 100 °C; (C) pH 7.3, 37 °C; and (D) pH 10.9, 37 °C. The inset in panel D shows the SAED pattern of the gold nanoparticles. The diffraction rings could be indexed as fcc gold. (E) UV−vis spectra of gold nanoparticles synthesized under different conditions: spectrum 1, pH 3.2 and 37 °C; spectrum 2, pH 3.2 and 70 °C; spectrum 3, pH 3.2 and 100 °C; spectrum 4, pH 7.3 and 37 °C; spectrum 5, pH 10.9 and 37 °C. The absorbance intensity of spectrum 1 has been multiplied tenfold.

reduction of chloroaurate ions and the attachment of the BSA chains to the gold surface, therefore producing smaller and more uniform gold nanoparticles as a result.

The large reddish brown nanoplates obtained at acidic pH settled slowly to the bottom of the flask when stirring was stopped. This was in strong contrast with the behavior of gold nanoparticle−BSA conjugates formed under neutral or alkaline condition where the hydrosol could remain stable for a month and more at room temperature. It is believed that the gold nanoparticles formed in the BSA solution were stabilized by a combination of Au−S bonding with the protein (via the 35 cysteine residues in BSA), and steric protection due to the bulkiness of the protein. This is consistent with the BSA stabilization of gold nanoparticles reported by Burt et al.[23] The larger size and lower dispersivity of gold nanoplates obtained under the acidic condition were the reason for precipitation.

It is expected that atoms on different crystallographic facets interacted differently with inorganic ions, polymeric or surfactant capping agents,[9] which could result in the anisotropic growth of a solid surface. The face-specific binding of proteins has been proposed for the protein-mediated controlled growth of calcium carbonate crystals.[24] We postulate that similar effects may also operate in the binding of BSA to the Au surface. Under the acidic condition, bulky BSA would preferentially adsorb on the {111} facets and consequently suppressed the growth in the ⟨111⟩ direction. Thus, anisotropic polygonal plates covered with {111} facets were formed. The recognition for specific facets was apparently lost at higher temperature (70 or 100 °C) and pH (neutral or alkaline). The exact mechanism for the face recognition property of BSA on gold surface under different temperature and pH is not clear at this time and the effects of protein sequence, size, conformation and charge on the face recognition property are still being investigated.

As a first attempt to gain further insights into the process, we analyzed the effect of pH on the charge of the protein molecule, which could help to shed some light on the identity of functional groups in BSA involved in the formation of gold nanoplates. The p*K*a of side groups of twenty amino acids is reproduced in Table S1.[25] Interestingly, of all the p*K*a of amino acid side groups, only the carboxyl groups in aspartic and glutamic acid residues have low p*K*a (3.71 and 4.15, respectively), while thiol and amine groups have high pKa (8.14 for cysteine and 10.67 for lysine). Therefore, an increase in pH from 3.2 to 7.3 would affect strongly the carboxyl groups, imparting

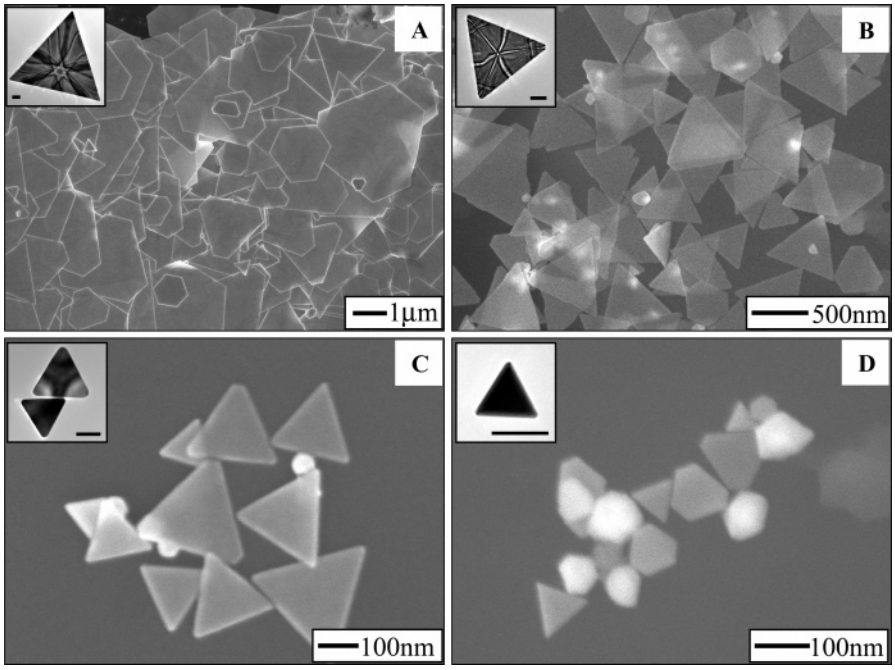

Figure 3. (A−D) Representative FESEM images of gold nanoplates synthesized in BSA solution with Ag^+ ion concentrations of 0, 1, 5, and 10 μM, respectively. The insets are high magnification TEM images. All scale bars are 100 nm.

them with negative charges through deprotonation. Considering the large amount of carboxyl groups in the BSA molecule (41 Asp and 58 Glu among the 583 amino acids making up BSA, or ~17% of all residues in BSA), the different charges on the protein molecule at different pH could affect the nature and the strength of interaction between the protein chains and the gold surface, leading to the formation of gold nanoparticles with different shapes at different pH (plate-like structures at pH 3.2 and spheres at pH 7.3). The carboxyl side groups (Asp and Glu) in the BSA molecule are believed to be primarily responsible for forming the plate-like gold nanostructures.

3. Size Manipulation of Gold Nanoplates. In addition to temperature and pH, we have found that the addition of a trace amount of Ag ions was able to significantly affect the reduction kinetics, and hence the lateral size of the nanoplates, without compromising the yield. Controlled experiments were carried out to determine the role of the Ag ions. It was found that Ag ions ($AgNO_3$) were reduced to Ag nanoparticles by BSA at 37 °C and in the absence of $AuCl_4^-$ ions (see Figure S2 for TEM, UV−vis and XPS analyses of the sample, which confirmed the formation of Ag nanoparticles). The reduction reaction was completed in 3h, which was much faster than the reduction of $AuCl_4^-$ by BSA (2 days). These Ag clusters, however, could be reoxidized to Ag^+ through a galvanic replacement reaction with the $AuCl_4^-$ ions.[26] The reactions may be categorically represented by eqs 1 to 3 below. Hence Ag^+ could serve as an electron relay to transfer electrons from the BSA chains to Au(III). The reduction kinetics of chloroaurate ions could therefore be changed by introducing different amounts of Ag^+ without affecting the capping and face recognition ability of BSA:

$$Ag^+ + BSA \xrightarrow{3\ h} Ag\ nanoparticles \quad (1)$$

$$AuCl_4^- + BSA \xrightarrow{48\ h} Au\ nanoparticles \quad (2)$$

$$AuCl_4^- + Ag(0) \rightarrow Au(0) + AgCl \quad (3)$$

Different quantities of aqueous silver nitrate solution were added to the mixture of 1 mM $HAuCl_4$ and 1 mg/mL BSA. Reactions were carried out under vigorous stirring in a water bath at 37 °C for 3−48 h. The results were also summarized in Table 1. When the concentration of Ag^+ was increased from 0 to 10 μM, the reduction time decreased from 48h to 6h. The average width (as measured by 100 triangular/hexagonal plates along their longest edges, see Figure 3A,D) of the nanoplates decreased from 2.1 μm to 91 nm. The faster reduction of chloroaurate ions in the presence of Ag^+ greatly increased the level of supersaturation and hence the number of seeds formed in the nucleation step; therefore, gold nanoplates with smaller sizes could be produced at the same gold precursor concentration. The lateral size of the nanoplates could be controlled within four size ranges with means of 2.1 μm, 590 nm, 205 nm, and 91 nm, respectively, by using different amounts of Ag^+. The reduction kinetics of chloroaurate ions was further increased (reaction completion in 3 h) at a Ag^+ concentration of 50 μM. However, the yield of the gold nanoplates was dramatically decreased to ~15%. In addition some distorted gold nanoplates were formed under this condition, as shown in Figure S3. These observations suggest the optimal concentration for Ag^+ was between 0 and 10 μM.

4. TEM Monitoring of the Growth of Gold Nanoplates in BSA Solution. The formation of the gold nanoplates was a slow process. Through time-course measurements we were able to follow the size and shape evolution of the product, as shown in Figure 4. A reaction mixture with 5 μM Ag^+ was selected because of its relatively fast reduction kinetics (reaction completion within 10 h) and a good yield of gold nanoplates (~60%).

The TEM image of the product sampled at 3 h is shown in Figure 4A, where tiny gold nanoparticles with size smaller than 2 nm populated densely on the surface of the TEM grid. Small triangular gold nanoparticles 3−20 nm in edge length (see arrows in Figure 4B) began to appear after the reaction mixture was aged for 5h. Jin et al.[9a] reported similar size (5−10 nm) of triangular-shaped Ag seeds formed in the early stages of their photoinduced conversion process. Between 5 and 10h of the reaction time, the size of the gold nanoplates grew while the edges became increasingly smoother. The growth of the gold nanoplates is reminiscent of gold nanoplate formation in

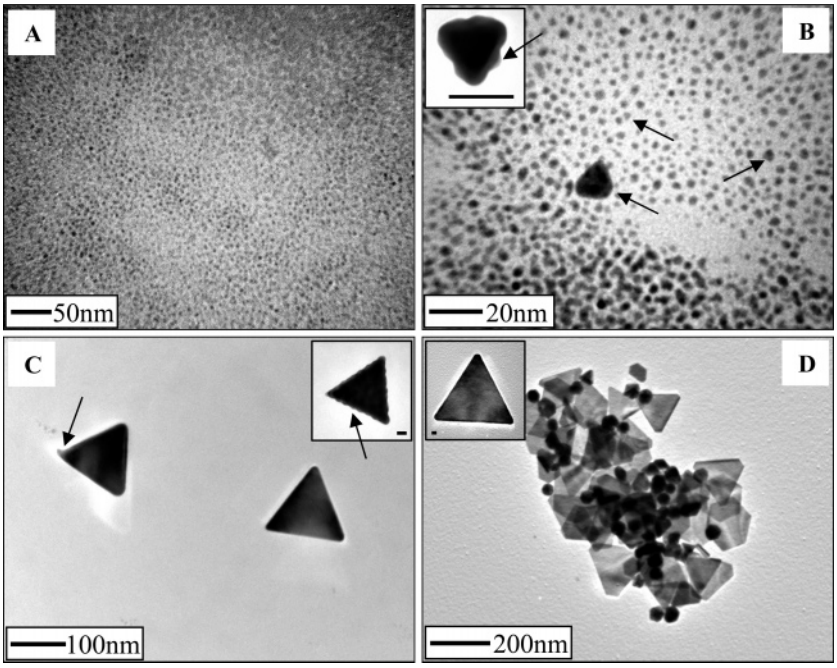

Figure 4. Representative TEM images of Au nanoparticles sampled at (A) 3, (B) 5, (C) 8, and (D) 10 h following the start of the reaction. Arrows in panel B show triangular-shaped seeds, and the arrow in the inset in panel B shows the corrugated structure of a growing gold nanoplate. Arrows in panel C show the attachment of gold nanoclusters on the active growth site of a gold nanoplate, and the arrow in the inset in panel C shows the steps formed on the growing surface of a gold nanoplate. All scale bars in the insets are 20 nm. Synthesis conditions: BSA (1 mL, 10 mg/mL) + deionized water (8 mL) + $HAuCl_4$ (1 mL, 10 mM) + $AgNO_3$ (5 μL, 10 mM); initial pH 3.2, 37 °C.

seaweed extract,[2] where the "surface wrapping" model of Zeng et al.[27] could be at work: Once a wrapping layer was established on the triangular-shaped seeds, it directed the growth of another layer, forming steps and corrugated edges in the process. The evidence for the attachment of gold nanoclusters to the active growth site of a particular triangular gold nanoparticle can be found in Figure 4C (see arrow). The presence of intermediate products with plate-like structures with corrugated and stepped edges can be clearly seen in the insets of Figure 4B,C (see arrows). With the increase in reaction time, the reaction rate decreased because of reactant depletion, and the deposition of gold would then follow the most energetically favorable path. The steps were leveled and the edges were smoothened (as shown in Figure 4D).

Conclusions

A simple one-pot synthesis, based on the biomineralization ability of BSA in aqueous solutions, was used to produce single-crystalline gold nanoplates with triangular and hexagonal shapes at good yield. Structural characterizations by FESEM, TEM, HRTEM, and SAED showed that the nanoplates were oriented with {111} planes as their basal planes. The effects of environmental factors such as temperature and pH were investigated, which showed that acidic pH and low temperature favored the anisotropic growth of gold nanoparticles. Ag^+ ions were introduced to modulate the kinetics of Au(III) reduction, and the lateral size of the Au nanoplates could then be controlled within several size ranges from a few μm to tens of nm. The growth of gold nanoplates in the serum albumin protein was reconstructed by following the changes in the TEM images with time. The reaction and products are important not only because they provide a biological route to the production of single crystalline gold nanoplates for a wide variety of applications, but also because they highlighted that the interaction between protein/peptide and gold ions/surface could be used advantageously as a green chemical alternative to the synthesis of nanogold. It is hoped that with continuing work on understanding the BSA-Au system, a green biomimetic synthesis may eventually be possible where rationally designed multifunctional peptides are used to produce nanomaterials with prescribed geometrical features, depending on the needs of the applications.

Acknowledgment. One of the authors (JP Xie) is financially supported by the Singapore−MIT Alliance (SMA) program.

Supporting Information Available: Amino acid composition of BSA and their corresponding pKa (side group); XPS analysis of gold nanoparticles synthesized by BSA at pH 3.2 and pH 10.9; TEM, UV−vis, and XPS analysis of silver nanoparticles synthesized by BSA at pH 3.2; TEM images of gold nanoparticles synthesized in BSA solution with introducing 50μM Ag^+ ions. This material is available free of charge via the Internet at http://pubs.acs.org.

References and Notes

(1) Raveendran, P.; Fu, J.; Wallen, S. L. *J. Am. Chem. Soc.* **2003**, *125*, 13940.

(2) Liu, B.; Xie, J.; Lee, J. Y.; Ting, Y. P.; Chen, J. P. *J. Phys. Chem. B* **2005**, *109*, 15256.

(3) (a) Song, Y.; Yang, Y.; Medforth, C. J.; Pereira, E.; Singh, A. K.; Xu, H.; Jiang, Y.; Brinker, C. J.; Swol, F. V.; Shelnutt, J. A. *J. Am. Chem. Soc.* **2004**, *126*, 635. (b) Raveendran, P.; Fu, J.; Wallen, S. L. *Green Chem.* **2006**, *8*, 34.

(4) (a) Burda, C.; Chen, X. B.; Narayanan, R.; El-Sayed, M. A. *Chem. Rev.* **2005**, *105*, 1025. (b) Liz-Marzan, L. M. *Langmuir* **2006**, *22*, 32. (c) Daniel, M. C.; Astruc, D. *Chem. Rev.* **2004**, *104*, 293.

(5) Murphy, C. J.; Sau, T. K.; Gole, A. M.; Orendorff, C. J.; Gao, J.; Gou, L.; Hunyadi, S. E.; Li, T. *J. Phys. Chem. B* **2005**, *109*, 13857.

(6) Zhou, Y.; Wang, C. Y.; Zhu, Y. R.; Chen, Z. Y. *Chem. Mater.* **1999**, *11*, 2310.

(7) (a) Chu, H. C.; Kuo, C. H.; Huang, M. H. *Inorg. Chem.* **2006**, *45*, 808. (b) Kan, C.; Zhu, X.; Wang, G. *J. Phys. Chem. B* **2006**, *110*, 4651. (c) Millstone, J. E.; Park, S.; Shuford, K. L.; Qin, L. D.; Schatz, G. C.; Mirkin, C. A. *J. Am. Chem. Soc.* **2005**, *127*, 5312.

(8) Shankar, S. S.; Rai, A.; Ankamwar, B.; Singh, A.; Ahmad, A.; Sastry, M. *Nat. Mater.* **2004**, *3*, 482.

(9) (a) Jin, R. C.; Cao, Y. W.; Mirkin, C. A.; Kelly, K. L.; Schatz, G. C.; Zheng, J. G. *Science* **2001**, *294*, 1901. (b) Jin, R. C.; Cao, Y. C.; Hao, E. C.; Métraux, G. S.; Schatz, G. C.; Mirkin, C. A. *Nature* **2003**, *425*, 487.

(10) M'etraux, G. S.; Mirkin, C. A. *Adv. Mater.* **2005**, *17*, 412.

(11) Tkachenko, A. G.; Xie, H.; Coleman, D.; Glomm, W.; Ryan, J.; Anderson, M. F.; Franzen, S.; Feldheim, D. L. *J. Am. Chem. Soc.* **2003**, *125*, 4700.

(12) Marcon, G.; Messori, L.; Orioli, P.; Cinellu, M. A.; Minghetti, G. *Eur. J. Biochem.* **2003**, *270*, 4655.

(13) Carter, D. C.; Ho, J. X. *Adv. Protein Chem.* **1994**, *45*, 153.

(14) Hirayama, K.; Akashi, S.; Furuya, M.; Fukuhara, K. L. *Biochem. Biophys. Res. Commun.* **1990**, *173*, 639.

(15) He, X. M.; Carter, D. C. *Nature* **1992**, *358*, 209.

(16) (a) Bhargava, S. K.; Booth, J. M.; Agrawal, S.; Coloe, P.; Kar, G. *Langmuir* **2005**, *21*, 5949. (b) Shao, Y.; Jin, Y. D.; Dong, S. J. *Chem. Commun.* **2004**, 1104.

(17) (a) Kirkland, A. I.; Jefferson, D. A.; Duff, D. G.; Edwards, P. P.; Gameson, I.; Johnson, B. F. G.; Smith, D. J. *Proc. R. Soc. London, Ser. A* **1993**, *440*, 589. (b) Germain, V.; Li, J.; Ingert, D.; Wang, Z. L.; Pileni, M. P. *J. Phys. Chem. B* **2003**, *107*, 8717. (c) Rodriguez-Gonzalez, B.; Pastoriza-Santos, I.; Liz-Marzan, L. M. *J. Phys. Chem. B* **2006**, *110*, 11796.

(18) (a) Auzary, S.; Pailloux, F.; Denanot, M. F.; Gaboriaud, R. J. *Thin Solid Films* **1998**, *319*, 163. (b) Yamanaka, J.; Nakamura, Y.; Nittono, O. *Mater. Sci. Eng., A* **1994**, *179*, 401.

(19) Mie, G. *Ann. Phys.* **1908**, *25*, 377.

(20) Cotton, F. A.; Wilkinson, G.; Murillo, C. A.; Bochmann, M. *Advanced Inorganic Chemistry*; Wiley-Interscience, New York, 1999; p 1101.

(21) (a) Henry, M. C.; Hsueh, C. C.; Timko, B. P.; Freund, M. S. *J. Electrochem. Soc.* **2001**, *148*, D155. (b) Liu, Y. C.; Chuang, T. C. *J. Phys. Chem. B* **2003**, *107*, 12383.

(22) Li, G. T.; Lauer, M.; Schulz, A.; Boettcher, C.; Li, F. T.; Fuhrhop, J. H. *Langmuir* **2003**, *19*, 6483.

(23) Burt, J. L.; Gutierrez-Wing, C.; Miki-Yoshida, M.; Jose-Yacaman, M. *Langmuir* **2004**, *20*, 11778.

(24) DeOliveira, D. B.; Laursen, R. A. *J. Am. Chem. Soc*. **1997**, *119*, 10627.

(25) *CRC Handbook of Chemistry and Physics*, 87th ed. electronic version; Chapman & Hall/CRC Press: Boca Raton, FL, 2006−2007.

(26) Sun, Y.; Mayers, B. T.; Xia, Y. *Nano Lett.* **2002**, *2*, 481.

(27) Feng, J.; Zeng, H. C. *Chem. Mater.* **2003**, *15*, 2829.